

Transition from soft- to hard-Pomeron in the structure functions of hadrons at small- x from holography

Akira Watanabe* and Katsuhiko Suzuki†

Department of Physics, Tokyo University of Science, Shinjuku, Tokyo 162-8601, Japan

(Dated: August 29, 2021)

Abstract

We study the nucleon and pion structure functions at small Bjorken- x region in the framework of holographic QCD with a special emphasis on the roles of AdS space wave functions. Using the BPST kernel for the Pomeron exchange and calculating its coupling to target hadrons in the AdS space, we obtain F_2 structure functions at the small- x . Results for the proton F_2^p as well as the pion F_2^π are consistent with experimental data of the deep inelastic scattering and the forward electroproduction of a neutron. Observed Q^2 dependence of the Pomeron intercept is well reproduced from soft non-perturbative ($Q^2 \sim 0$) to hard perturbative ($Q^2 \gg 1\text{GeV}^2$) region. We find the interplay between soft and hard Pomerons is closely related with behavior of AdS wave functions of hadrons and the virtual photon.

PACS numbers: 11.25.Tq, 13.60.Hb, 12.40.Nn

Keywords: gauge/gravity correspondence, Pomeron, deep inelastic scattering

* j1210709@ed.tus.ac.jp

† katsu_s@rs.kagu.tus.ac.jp

I. INTRODUCTION

The structure functions of hadrons $F_2(x, Q^2)$ at the small Bjorken- x region provide unique opportunities to access the gluon dynamics of QCD. At $x \leq 10^{-2}$, the structure function is dominated by the gluon contribution, which may be identified with the Pomeron in QCD [1]. Within the Regge theory, the elastic (or diffractive) forward scattering amplitude is described by the exchange of the vacuum quantum number, which is so called Pomeron. Assuming the Pomeron exchange with α_0 and α' being constants, one can write a two-body scattering amplitude as

$$\mathcal{A}(s, t) \sim s^{\alpha_0 + \alpha' t}, \quad (1)$$

where the energy \sqrt{s} and the momentum transfer t satisfy the Regge kinematics $s \gg t$. Thus, the total cross section is expressed by

$$\sigma(s) \sim s^{\alpha_0 - 1}, \quad (2)$$

which indicates the cross section of the high energy scattering depends on a single parameter α_0 , Pomeron intercept.

Phenomenologically, hadron-hadron collision as well as photon-hadron scattering at high energies are described very well by the ‘soft’ Pomeron intercept $\alpha_0 \sim 1.1$ [2]. However, some hard scale Q enters into the process, situation becomes different. For example, in the deep inelastic scattering (DIS) off the nucleon with the photon virtuality Q^2 , the Pomeron exchange model leads to a form of the structure function F_2 as

$$F_2(x, Q^2) \sim x^{1 - \alpha_0}, \quad (3)$$

which is valid for the small Bjorken- x , $x = Q^2/s \ll 1$. In this hard process, the experimental data [3] is consistent with the ‘hard’ intercept $\alpha_0 \sim 1.4$ for $Q^2 \gg 1\text{GeV}^2$ in contrast to the soft Pomeron value $\alpha_0 \sim 1.1$. This large value of the intercept is rather consistent with the BFKL Pomeron, which is the Reggeized two gluon exchange calculated by perturbative QCD [4]. Hence, it is reasonable to conclude that the Pomeron intercept depends on the scale of the scattering process, $\alpha_0(Q)$, where the scale Q means, *e.g.* photon virtuality, quark mass, or momentum transfer. Indeed, similar scale dependence is observed in the diffractive photoproduction of light and heavy vector mesons [5].

Although we have a clear signal of the transition between ‘soft’ and ‘hard’ Pomerons, we cannot calculate such a scale dependence theoretically, because it is extremely hard to obtain the soft Pomeron as a solution of the non-perturbative QCD. Recently, the holographic description of QCD has gathered theoretical interests as a tool to calculate the non-perturbative quantities in QCD. Using the AdS/CFT correspondence (or gauge/gravity in general), one may relate the strong coupling gauge theory at the boundary with the classical theory of the gravitation in the bulk AdS space in the large ’t Hooft coupling limit [6–8]. According to the AdS/CFT dictionary, the holographic description of QCD may be achieved by the top down approach which originates from the string theory in the higher dimensional space [9], or more phenomenological bottom up approach [10, 11]. The holographic models are applied to phenomenological studies successfully [9, 12–14].

The first study of the Pomeron with the gauge/gravity correspondence was done in Ref. [15]. Later, much elaborated studies have been done in Refs. [16–18]. In those studies, the Brower-Polchinski-Strassler-Tan (BPST) kernel which represents the Pomeron exchange in the AdS space is introduced based on the string theory to describe Q^2 dependence of the Pomeron intercept. In Ref. [18], the authors calculated the nucleon structure function at the small- x with the ‘super local approximation’, in which overlap functions (probability distributions in the AdS space) of the photon and the nucleon are simply replaced with delta functions. The results are in good agreement with the data, although the validity of this approximation seems to be unclear.

In this paper, we shall calculate the nucleon structure function at the small- x based on the BPST Pomeron kernel without resorting the ‘super local approximation’. To do so we use the AdS wave functions of hadrons calculated from holographic QCD, and obtain their coupling to the Pomeron in the AdS space. Methods to deal with the nucleon properties have been already developed and can be applied to the Pomeron exchange. We demonstrate a ‘consistent’ holographic description of the structure function, by calculating the Pomeron kernel, wave functions of scattering particles, and the Pomeron-hadron-hadron three point function, gives excellent results for the small- x structure function without any artificial assumptions.

In addition, we calculate the pion structure function at the small- x in the same way. We find $F_2^\pi(x)$ at the small- x is suppressed compared with the nucleon case. In spite of the lack of the DIS data for the pion, one can extract (model dependent) information on the pion

structure function from the forward electro-production of a neutron $e + p \rightarrow e' + n + X$ with a large rapidity gap [19]. Our calculations are in good agreement with the existing data.

This paper is organized as follows. In Sec. II, we introduce the BPST kernel and discuss its properties with the delta function approximation for the overlap functions. We show why behavior of the AdS wave functions is important to reproduce the scale dependence of the effective Pomeron intercept. Sec. III is devoted to the short review of calculating the wave functions of hadrons and their couplings with the Pomeron in the holographic QCD. We show numerical results for the proton structure function in Sec. IV. In Sec. V, we calculate the pion structure function and compare it with the existing parameterizations and the data of the forward neutron production at HERA. Final section is devoted to the summary and discussions.

II. BPST KERNEL FOR POMERON EXCHANGE IN ADS SPACE

We first introduce the kernel in the AdS space for the Pomeron exchange, and discuss its properties in some detail. We assume the two-body scattering amplitude \mathcal{A} for a process $1 + 2 \rightarrow 3 + 4$ at the high energy is given by [15–17]

$$\mathcal{A}(s, t) = 2is \int d^2b e^{i\mathbf{k}_\perp \cdot \mathbf{b}} \int dz dz' P_{13}(z) P_{24}(z') \{1 - e^{i\chi(s, \mathbf{b}, z, z')}\} , \quad (4)$$

where s is the invariant mass square $s = (p_1 + p_2)^2$, and t the momentum transfer $t = (p_1 - p_2)^2$. This expression is valid for the near-forward scattering with a condition $s \gg t$, and is dominated by the Pomeron exchange. The impact parameter \mathbf{b} is the transverse vector perpendicular to the forward direction. The BPST Pomeron exchange kernel is expressed as the eikonal form $1 - e^{i\chi(s, \mathbf{b}, z, z')}$. $P_{13}(z)$ and $P_{24}(z')$ are overlap functions of incoming and outgoing particles with their 5D-coordinates z and z' . Physically, the overlap functions stand for the density distribution functions of participants in the AdS space, as we will see later.

We concentrate on the deep inelastic scattering in this work. Thus, it is enough to consider the virtual photon γ^* ($1 = 3 = \gamma^*$) with the virtuality Q^2 and the nucleon ($2 = 4 = N$) in the forward limit $t = 0$. Using the optical theorem and keeping the leading contribution in the eikonal approximation for the kernel, we write the structure function at the small

$x = Q^2/s$ as

$$F_2(x, Q^2) = \frac{Q^2}{2\pi^2} \int d^2b \int dzdz' P_{13}(z, Q^2) P_{24}(z') \text{Im}\chi(s, \mathbf{b}, z, z'), \quad (5)$$

where the imaginary part of the BPST kernel is given by

$$\text{Im}\chi(s, \mathbf{b}, z, z') = \frac{g_0^2}{16\pi} \sqrt{\frac{\rho}{\pi}} e^{(1-\rho)\tau} \frac{\xi}{\sinh \xi} \frac{\exp(\frac{-\xi^2}{\rho\tau})}{\tau^{3/2}}, \quad (6)$$

where

$$\tau = \log(\rho z z' s/2), \quad (7)$$

$$\xi = \sinh^{-1} \left(\frac{b^2 + (z - z')^2}{2zz'} \right). \quad (8)$$

Here, g_0^2 and ρ are the parameters of the model, which are specified later. Carrying out the integration over \mathbf{b} analytically, one finds

$$\int d^2b \text{Im}\chi(s, \mathbf{b}, z, z') = \frac{g_0^2}{16} \sqrt{\frac{\rho^3}{\pi}} (zz') e^{(1-\rho)\tau} \frac{\exp(\frac{-(\log z - \log z')^2}{\rho\tau})}{\tau^{1/2}}. \quad (9)$$

Hence, one can write down an expression for $F_2(x, Q^2)$ as

$$F_2(x, Q^2) = \frac{g_0^2 \rho^{3/2}}{32\pi^{5/2}} \int dzdz' P_{13}(z, Q^2) P_{24}(z') (zz' Q^2) e^{(1-\rho)\tau} \frac{\exp(\frac{-(\log z - \log z')^2}{\rho\tau})}{\tau^{1/2}}. \quad (10)$$

The expression (10) is obtained within the conformal field theory. However, we need some energy (or length) scale which breaks the conformal invariance to reproduce realistic QCD in the 4-dimension. One of the simplest choices to break the conformal symmetry is to introduce the sharp cutoff for the AdS coordinate z . The ‘hard-wall’ model with a sharp cutoff z_0 provides with a confinement and a mass gap of the hadron spectrum for the holographic QCD. This model has been applied successfully to calculations of various observables of QCD [12].

Inclusion of the hard-wall in the BPST kernel is already considered [18], by the following simple substitution of the Pomeron exchange kernel, $\chi_c \rightarrow \chi_{\text{hw}}$,

$$\text{Im}[\chi_c(s, z, z')] \equiv e^{(1-\rho)\tau} e^{-\frac{\log^2 z/z'}{\rho\tau}} / \tau^{1/2}, \quad (11)$$

$$\text{Im}[\chi_{\text{hw}}] \equiv \text{Im}[\chi_c] + \mathcal{F}(z, z', \tau) \text{Im}[\chi_c(s, z, z_0 z'_0/z')], \quad (12)$$

$$\mathcal{F}(z, z', \tau) = 1 - 2\sqrt{\rho\pi\tau} e^{\eta^2} \text{erfc}(\eta),$$

$$\eta = \left(-\log \frac{zz'}{z_0 z'_0} + \rho\tau \right) / \sqrt{\rho\tau},$$

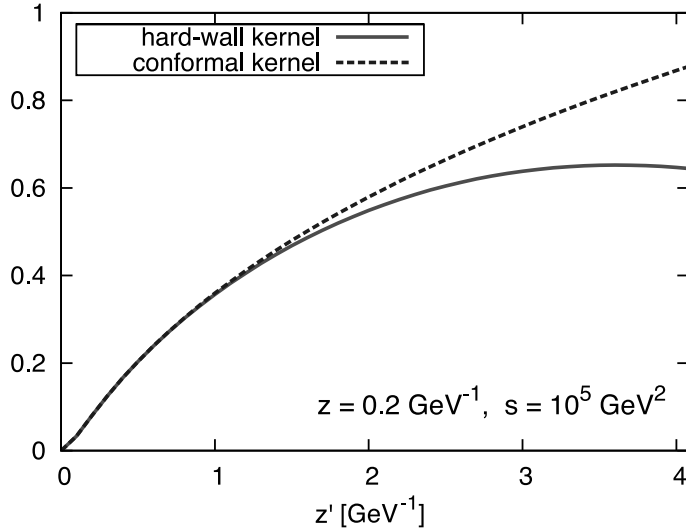


FIG. 1. Comparison of BPST kernel. The solid and dashed curves indicate the hard-wall and conformal kernels, respectively. Here, we use $\rho = 0.77$.

where z_0 is the hard-wall parameter. With this substitution, F_2 now has a form

$$F_2(x, Q^2) = \frac{g_0^2 \rho^{3/2}}{32\pi^{5/2}} \int dz dz' P_{13}(z, Q^2) P_{24}(z')(zz'Q^2) \text{Im}[\chi_{\text{hw}}] . \quad (13)$$

To study qualitative difference between the conformal (11) and hard-wall kernel (12), we show in Fig. 1 $\text{Im}[\chi_c]$ and $\text{Im}[\chi_{\text{hw}}]$ as a function of z' with the $z = 0.2\text{GeV}^{-1}$ (typical value of z for the virtual photon overlap function P_{13}). While both Pomeron kernels show the same behavior around small z' , the hard-wall model deviates from the conformal one for $z' \sim 3\text{GeV}^{-1} \sim 0.6\text{fm}$, which may correspond to a typical size of the hadrons. Later, we show numerical results of both hard-wall and conformal cases to discuss the role of the hard-wall boundary.

The advantage of the use of the BPST kernel is to incorporate the correct scale dependence of the Pomeron intercept [15–17]. As we have discussed in the Introduction, the Pomeron intercept α_0 is close to 1 for the soft hadronic interaction. When the hard scale appears in the process like DIS, α_0 increases up to about 1.4. Therefore, it is important to discuss how the energy scale of the process changes the Pomeron intercept in this model.

In order to see such properties of the Pomeron kernel, it is convenient to adopt ‘super local approximation’ for the overlap functions [18]. The ‘super local’ ansatz is nothing but the delta function approximation for the distribution functions in the AdS space,

$$P_{13}(z, Q^2) \approx \delta(z - 1/Q) , \quad P_{24}(z') \approx \delta(z' - 1/Q') , \quad (14)$$

where Q and Q' may be understood as the typical energy scales of the incident and target particles. Thus, for DIS, Q and Q' may be identified with the virtual photon momentum and the mass of the target hadron, respectively.

Inserting them into (10) one obtains (here we consider only the conformal case for simplicity.)

$$F_2(x, Q^2) \propto \frac{Q}{Q'} \times \frac{x^{\rho-1}}{(-\log x)^{1/2}} \times \exp\left(\frac{(\log \frac{Q}{Q'})^2}{\rho \log x}\right). \quad (15)$$

In Eq. (15) the Bjorken- x dependence mainly comes from a term $x^{\rho-1}/(-\log x)^{1/2}$, which is independent of Q, Q' . The subtle Q, Q' dependences arise from the last exponential factor $\exp\left(\log^2 \frac{Q}{Q'}/\rho \log x\right)$. Fig. 2 shows the x -dependences of Eq. (15) for several values of Q, Q' . With $Q/Q' = 1$ it shows rather weak x dependence, where the resulting Pomeron intercept is small, $\alpha_0 \sim 1.1$. If we set $Q/Q' = 20$, the BPST kernel increases rapidly as x decreasing, giving the large intercept, $\alpha_0 \sim 1.4$. This striking change is due to $\log(Q/Q')$ factor in the exponential factor shown in Fig. 2. Hence, in order to require that the BPST kernel is capable of describing the ‘soft’ to ‘hard’ transition of the Pomeron, Q/Q' must be large for the hard process, while $Q/Q' \sim 1$ for the soft process.

In the super local approximation, $1/Q, 1/Q'$ are simply related with positions of the delta function peak for $P_{13}(z)$ and $P_{24}(z')$. For example, if we want to acquire the large Pomeron intercept, we need a ‘gap’ between the peak positions of the overlap functions of the virtual photon and the nucleon, namely, $P_{13}(z)$ must have a sharp peak at $z \sim 0$, which is far away from the distribution of $P_{24}(z')$ in the AdS space. In the next section we introduce the AdS wave functions for the nucleon and pion, and calculate their overlap functions. We show such a ‘gap’ in the AdS space between P_{13} and P_{24} naturally incorporated within the holographic QCD as the scale Q^2 increases.

III. HADRONIC WAVE FUNCTIONS IN ADS SPACE AND POMERON COUPLING

In order to calculate Eqs. (10) and (13) we need evaluate the hadronic wave functions in the AdS space in terms of the holographic QCD. For the virtual photon, we use the massless 5D U(1) vector field [18, 20–22], which is dual to the electromagnetic current. This vector fields satisfy the Maxwell equation in the bulk AdS space. The overlap function of

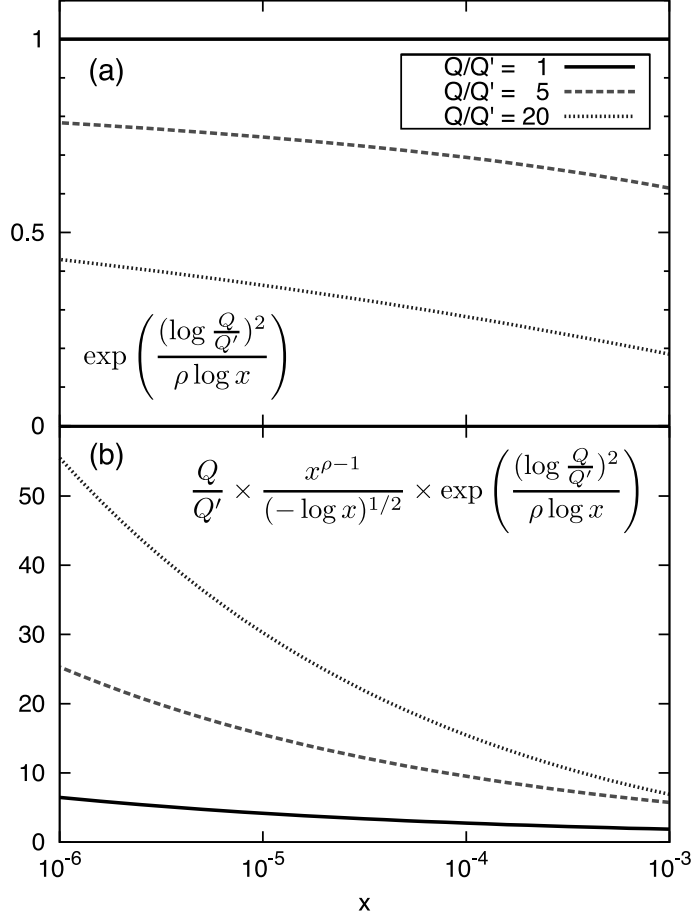


FIG. 2. F_2 with the delta function approximation for the wave functions. (a) Last exponential factor in Eq. (15) as a function of x for Q/Q' . (b) F_2 for $Q/Q' = 1, 5, 20$.

the virtual photon is found to be [18]

$$P_{13}(z, Q^2) = \frac{1}{z} (Qz)^2 (K_0^2(Qz) + K_1^2(Qz)) . \quad (16)$$

This function in the AdS space basically corresponds to the photon impact factor in QCD.

On the other hand, we adopt the hadronic wave functions calculated in the AdS space with the metric,

$$ds^2 = g_{MN} dx^M dx^N = \frac{1}{z^2} (\eta_{\mu\nu} dx^\mu dx^\nu - dz^2) . \quad (17)$$

We consider the hard-wall model $\varepsilon \leq z \leq z_0$ ($\varepsilon \rightarrow 0$) in the following calculation where IR boundary z_0 breaks the conformal symmetry to mimic the realistic QCD. Hereafter, we briefly review the calculations of the AdS wave functions in the holographic QCD.

For the nucleon case, we use the model of Refs. [23–26, 30] in which the nucleon is described by a solution of the 5-dimensional Dirac equation. The classical action for the

Dirac field is given by

$$S_F = \int d^5x \sqrt{g} \left(\frac{i}{2} \bar{\Psi} e_A^N \Gamma^A D_N \Psi - \frac{i}{2} (D_N \Psi)^\dagger \Gamma^0 e_A^N \Gamma^A \Psi - M \bar{\Psi} \Psi \right), \quad (18)$$

where $e_A^N = z \delta_A^N$ and $D_N = \partial_N + \frac{1}{8} \omega_{NAB} [\Gamma^A, \Gamma^B] - iV_N$ are introduced to maintain the invariance of the action under the gauge transformation and generalized coordinate transformation in the AdS space. The mass of the spinor is $M = 3/2$ by the AdS/CFT dictionary. Ψ is obtained as a solution of the Dirac equation,

$$(ie_A^N \Gamma^A D_N - M) \Psi = 0. \quad (19)$$

To derive this equation we require a boundary condition at the hard-wall, either $\Psi_R(z_0) = 0$ or $\Psi_L(z_0) = 0$, where we define the right- and left-handed spinor; $\Psi_{R,L} = (1/2)(1 \pm \gamma^5)\Psi$.

Carrying out the Fourier transform in the 4-dimensional space with a momentum p^μ , one can express the Dirac field as

$$\Psi_{R,L}(p, z) = z^\Delta \Psi_{R,L}^0(p) f_{R,L}(p, z),$$

where $\Psi_{R,L}^0(p)$ is a plane wave solution in the 4-dimensional space which plays a role of the source field for the spin-1/2 baryon operator, and $f_{R,L}(p, z)$ the bulk-to-boundary propagator. Δ is chosen to satisfy a condition $f(p, \varepsilon) = 1$.

Dropping the interaction term with the gauge field, one can rewrite the Dirac equation as,

$$\begin{aligned} \left(\partial_z - \frac{2 + M - \Delta}{z} \right) f_R &= -p f_L, \\ \left(\partial_z - \frac{2 - M - \Delta}{z} \right) f_L &= p f_R, \end{aligned} \quad (20)$$

where $p = \sqrt{p^2}$. Imposing a condition that solutions are not singular at $z = \varepsilon$, we require $\Delta = 2 - M$.

Choosing the boundary conditions $f_R(z_0) = 0$ and $f_L(\varepsilon) = 1$, one finds normalizable modes $\psi_L(z) = f_L(p = m_n^N, z)$ and $\psi_R(z) = f_R(p = m_n^N, z)$ from Eqs. (20) with m_n^N being the mass of the n -th Kaluza-Klein state;

$$\psi_L^{(n)}(z) = \frac{\sqrt{2} z^\alpha J_\alpha(m_n^N z)}{z_0 J_\alpha(m_n^N z_0)}, \quad \psi_R^{(n)}(z) = \frac{\sqrt{2} z^\alpha J_{\alpha-1}(m_n^N z)}{z_0 J_\alpha(m_n^N z_0)}. \quad (21)$$

Here, $\alpha = M + \frac{1}{2}$ and the eigenvalue m_n^N is determined by the boundary condition at IR boundary, $J_{\alpha-1}(m_n^N z_0) = 0$. The hard-wall parameter z_0 is fixed to reproduce the nucleon mass as the lowest eigenstate. These solutions are subject to the normalization conditions,

$$\int dz \frac{1}{z^3} \psi_L^{(n)} \psi_L^{(m)} = \int dz \frac{1}{z^3} \psi_R^{(n)} \psi_R^{(m)} = \delta_{nm} . \quad (22)$$

On the other hand, we adopt the pion wave function studied in Ref. [11], which will be sketched below. This wave function is successfully applied to the calculation of dynamical quantities of the pion, *e.g.* electromagnetic form factor [27, 28] or anomalous $\pi^0 \rightarrow \gamma\gamma$ transition [29]. The effective action for the meson fields is

$$S_M = \int d^5x \sqrt{g} \left[\text{Tr} \left\{ |DX|^2 + 3|X|^2 - \frac{1}{4g_5^2} (F_L^2 + F_R^2) \right\} \right] , \quad (23)$$

where the covariant derivative $D^M X = \partial^M X - iA_L^M X + iX A_R^M$ is introduced with the gauge field A_L^M, A_R^M , and $F_{L,R}^{MN} = \partial^M A_{L,R}^N - \partial^N A_{L,R}^M - i[A_{L,R}^M, A_{L,R}^N]$, the field strength tensor. The bulk field X is defined by $X(x, z) = X_0(z) \exp(2it^a \pi^a)$ with the bulk scalar X_0 and the pion field π^a with the isospin operator t^a . The bulk scalar is given by

$$X_0 = \frac{1}{2} \mathbb{I} v(z) = \frac{1}{2} \mathbb{I} (m_q z + \sigma z^3) , \quad (24)$$

where m_q can be identified with the quark mass and σ the chiral condensate. Hereafter, we take the chiral limit, $m_q = 0$, for simplicity, and the pion is always massless.

Up to the second order of the fields, the action for the pion π and the axial-vector field $A = (A_L - A_R)/2$ is

$$S_A = \int d^5x \sqrt{g} \left[\frac{v(z)^2}{2} g^{MN} (\partial_M \pi^a - A_M^a) (\partial_N \pi^a - A_N^a) - \frac{1}{4g_5^2} g^{KL} g^{MN} F_{KM}^a F_{LN}^a \right] . \quad (25)$$

We work with the gauge fixing condition $A_z = 0$ for the axial-vector field. The axial vector field can be expressed as $A_\mu^a = A_{\mu\perp}^a + A_{\mu\parallel}^a$, where $A_{\mu\perp}^a$ and $A_{\mu\parallel}^a$ are the transverse and longitudinal components. The longitudinal part $A_{\mu\parallel}^a = \partial_\mu \phi^a$ contributes to the Goldstone mode due to the spontaneous chiral symmetry breaking.

Applying the Fourier transform with a momentum q , we decompose A_\perp, ϕ, π fields into sources in the 4-dimension and the bulk-to-boundary propagators $A(q, z)$, $\phi(q, z)$, and

$\pi(q, z)$. One obtains classical equations of motion for the pion sector as

$$\partial_z \left(\frac{1}{z} \partial_z A(q, z) \right) + \frac{q^2}{z} A(q, z) - \frac{g_5^2 v^2}{z^3} A(q, z) = 0, \quad (26)$$

$$\partial_z \left(\frac{1}{z} \partial_z \phi(q, z) \right) + \frac{g_5^2 v^2}{z^3} (\pi(q, z) - \phi(q, z)) = 0, \quad (27)$$

$$-q^2 \partial_z \phi(q, z) + \frac{g_5^2 v^2}{z^2} \partial_z \pi(q, z) = 0. \quad (28)$$

We look for solutions of Eqs. (26,27,28), which satisfy the boundary conditions, $\phi(0) = 0$, $\partial_z \phi(z_0) = 0$, and $\pi(0) = 0$ [11]. In addition, $\pi(z)$ must approach -1 away from $z = \varepsilon$ to recover the Gell-Mann–Oakes–Renner relation [11]. On the other hand, the bulk-to-boundary propagator of the transverse axial-vector field $A(q, z)$ is subject to $A(q, \varepsilon) = 1$ and $\partial_z A(q, z_0) = 0$.

Since we consider the massless pion in the chiral limit, $m_\pi^2 = q^2 = 0$, we obtain $\pi(0, z) = -1$ from Eq. (28) and the boundary condition. In this case, Eq. (27) coincides with Eq. (26), giving a relation $\phi(0, z) = A(0, z) - 1 = A(0, z) + \pi(0, z)$. Thus, it is convenient to introduce the new wave function of the pion, $\Psi(z) \equiv \phi(z) - \pi(z) = A(z)$ [28]. We write the equation for Ψ from Eq. (27),

$$z^3 \partial_z \left(\frac{1}{z} \partial_z \Psi \right) - g_5^2 v^2 \Psi = 0, \quad (29)$$

which leads to a solution,

$$\Psi(z) = z\Gamma \left[\frac{2}{3} \right] \left(\frac{\beta}{2} \right)^{1/3} \left[I_{-1/3}(\beta z^3) - I_{1/3}(\beta z^3) \frac{I_{2/3}(\beta(z_0^\pi)^3)}{I_{-2/3}(\beta(z_0^\pi)^3)} \right], \quad (30)$$

with $\beta = 2\pi\sigma/3$.

On the other hand, one can relate $A(0, z)$ with the pion decay constant f_π , defined by $\langle 0 | A_\mu | \pi(q) \rangle = i f_\pi q_\mu$. Calculation of the axial-current correlator based on the holographic principle yields,

$$f_\pi^2 = - \frac{1}{g_5^2} \frac{\partial_z A(0, z)}{z} \Big|_\varepsilon. \quad (31)$$

The model parameters σ and IR hard-wall z_0 can be determined to reproduce the ρ meson mass and the pion decay constant [11]. The gauge coupling g_5 is fixed by the matching condition at the UV boundary $z = \varepsilon$.

In order to calculate the Pomeron coupling with the hadrons, we consider the hadron-graviton-hadron three point function [30, 31]. To do so, we introduce the perturbation to

the metric $\eta_{\mu\nu} \rightarrow \eta_{\mu\nu} + h_{\mu\nu}$ in the classical action, and extract hAA terms, which contribute to the three point function.

First we determine behavior of $h_{\mu\nu}$ itself by solving the equation of motion. Introducing the 4-momentum q for $h_{\mu\nu}$ after the Fourier transform, we write $h_{\mu\nu}(q, z) = h_{\mu\nu}^0(q)H(Q, z)$ with $Q = \sqrt{-q^2}$. By virtue of the transverse-traceless gauge, $\partial^\mu h_{\mu\nu} = 0$ and $h^\mu{}_\mu = 0$, the linearized Einstein equation for the bulk-to-boundary propagator $H(Q, z)$ is

$$\left[\partial_z \left(\frac{1}{z^3} \partial_z \right) + \frac{1}{z^3} q^2 \right] H(Q, z) = 0. \quad (32)$$

Imposing the conditions, $\partial_z H(Q, z_0) = 0$ and $H(Q, \varepsilon) = 1$, we obtain

$$H(Q, z) = \frac{1}{2} Q^2 z^2 \left[\frac{K_1(Qz_0)}{I_1(Qz_0)} I_2(Qz) + K_2(Qz) \right], \quad (33)$$

which satisfies $H(\varepsilon, z) = 1$ as expected [30, 31].

As an example, we will review the pion case following the work of Ref. [31]. The three point function of the stress tensor with the axial currents can be calculated as,

$$\langle 0 | \mathcal{T} J_5^{a\alpha}(x) \hat{T}_{\mu\nu}(y) J_5^{b\beta}(w) | 0 \rangle = \frac{-2\delta^3 S}{\delta A_\alpha^{a0}(x) \delta h^{\mu\nu 0}(y) \delta A_\beta^{b0}(w)}. \quad (34)$$

To calculate the RHS of Eq. (34) from the classical action Eq. (25), we extract terms which are linear in $h_{\mu\nu}$ and quadratic in π and A ;

$$S_A^{(3)} = \int d^5 x \left[-\frac{v(z)^2 h^{\rho\sigma}}{2z^3} (\partial_\rho \pi^a - A_\rho^a) (\partial_\sigma \pi^a - A_\sigma^a) + \frac{1}{2g_5^2 z} h^{\rho\sigma} [-F_{\sigma z} F_{\rho z} + \eta^{\alpha\beta} F_{\sigma\alpha} F_{\rho\beta}] \right]. \quad (35)$$

On the other hand, the LHS of Eq. (34) in the momentum space is rewritten with the matrix element of the stress tensor between the pion states $\langle \pi^a(p_2) | \hat{T}^{\mu\nu} | \pi^b(p_1) \rangle$, by inserting the intermediate states (pion) and using $\langle 0 | A_\mu | \pi(p) \rangle = i f_\pi p_\mu$ with $p_1^2, p_2^2 \rightarrow 0$ [31]. From the symmetry consideration, the matrix element of the stress tensor between the pion states can be parameterized by

$$\langle \pi^a(p_2) | \hat{T}^{\mu\nu} | \pi^b(p_1) \rangle = 2\delta^{ab} F_\pi(\ell^2) [(p_1 + p_2)^\mu (p_1 + p_2)^\nu + \dots], \quad (36)$$

where $\ell = p_2 - p_1$, and F_π determines the magnitude of the matrix element. Here, we only retain the dominant contribution in the small- x kinematics, $p_1, p_2 \gg \ell$.

Functional differentiation of Eq. (34) with Eqs. (35,36) gives

$$F_\pi(\ell^2) = \int_\varepsilon^{z_0} dz H(\ell^2, z) \left[\frac{(\partial_z \Psi(z))^2}{g_5^2 f_\pi^2 z} + \frac{v(z)^2 \Psi(z)^2}{f_\pi^2 z^3} \right]. \quad (37)$$

In the case of DIS, it is enough to consider the forward limit $\ell = 0$, at which $H(\varepsilon, z) = 1$. Hence, the overlap function P_{24} for the pion is identified with

$$P_{24}^\pi(z) = \left[\frac{(\partial_z \Psi(z))^2}{g_5^2 f_\pi^2 z} + \frac{v(z)^2 \Psi(z)^2}{f_\pi^2 z^3} \right]. \quad (38)$$

We note that the overlap function Eq. (38) satisfies the normalization condition; $\int_\varepsilon^{z_0} dz P_{24}^\pi(z) = 1$. One can check it by integrating by parts,

$$\begin{aligned} & \int_\varepsilon^{z_0} dz \left[\frac{(\partial_z \Psi(z))^2}{g_5^2 f_\pi^2 z} + \frac{v(z)^2 \Psi(z)^2}{f_\pi^2 z^3} \right] \\ &= \left[\Psi(z) \frac{\partial_z \Psi(z)}{g_5^2 f_\pi^2 z} \right]_\varepsilon^{z_0} - \int_\varepsilon^{z_0} dz \left[\frac{\Psi(z)}{g_5^2 f_\pi^2 z^3} \left\{ z^3 \partial_z \left(\frac{\partial_z \Psi(z)}{z} \right) - g_5^2 v^2 \Psi(z) \right\} \right] \\ &= 1, \end{aligned} \quad (39)$$

where we use Eqs. (29) and (31), and the boundary conditions $\partial_z \Psi(z_0) = 0$. We also note that $P_{24}(z)$ can be understood as the probability density distribution in the bulk coordinate space, although the expression of Eq. (38) involves derivative of the wave function and differs from the familiar Ψ^2 form. However, the expression Eq. (38) also appears in the calculations of the pion electromagnetic form factor [27, 28] and the $\pi\pi\rho$ coupling constant [11]. In fact, the expression of Eq. (38) depends on the choice of the gauge. Alternative gauge fixing condition provides a familiar wave function square form [32].

One can apply the similar method to the nucleon case [30], and find P_{24}^N as

$$P_{24}^N(z) = \frac{1}{2z^3} (\psi_L^2(z) + \psi_R^2(z)). \quad (40)$$

This is apparently interpreted as the density distribution and fulfills the normalization condition [30],

$$\int_\varepsilon^{z_0} dz P_{24}^N(z) = 1, \quad (41)$$

with the help of the wave function normalization Eq. (22).

We show in Fig. 3 the hadronic overlap functions $zP_{24}^N(z)$ and $zP_{24}^\pi(z)$, as appeared in the formulae of the Pomeron scattering amplitudes, Eqs. (10) and (13). Both the nucleon and pion cases show similar z -dependences, whose peak positions are located near the hard-wall cutoff z_0 .

In Fig. 3, the overlap functions of the virtual photon $P_{13}(z, Q^2)$ with $Q^2 = 0.1, 1$, and 10GeV^2 are also shown to compare with the nucleon and the pion counterparts. It is important to note that shape of the photon overlap function drastically changes as the photon virtuality increases.

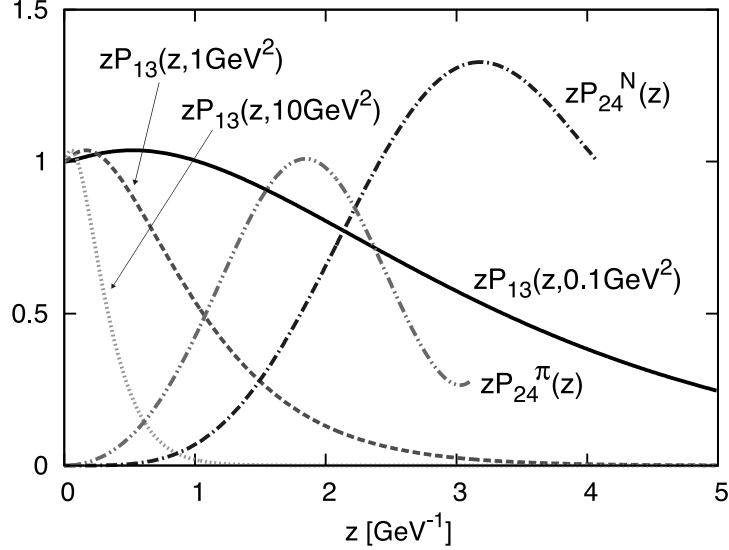


FIG. 3. The overlap functions in the integrand of Eqs. (10) and (13). The solid, dashed, and dotted curves indicate $zP_{13}(z, Q^2)$ with $Q^2 = 0.1\text{GeV}^2$, 1GeV^2 and 10GeV^2 , respectively. $P_{24}(z)$ for the nucleon is shown by the dashed-dotted curve, and one for the pion by the dashed double-dotted curve.

In Sec. II we have shown the Pomeron intercept α_0 becomes large (hard value) only if the distribution of the photon overlap function, $P_{13}(z)$, substantially differs from that of the target, $P_{24}(z')$. Here, using the realistic AdS wave functions, we find such a condition is in fact realized only at the larger $Q^2 \sim 10\text{GeV}^2$ region, where P_{13} shows a sharp peak at $z \sim 0$. On the other hand, Fig. 3 tells us that the photon overlap function at lower $Q^2 \leq 1\text{GeV}^2$ extends over the entire z region. Thus, the resulting Pomeron intercept may become smaller according to the discussion in Sec. II. In the next section we shall demonstrate how the Pomeron intercept $\alpha_0(Q^2)$ changes as the scale Q^2 increases by the numerical calculation.

IV. NUMERICAL RESULTS FOR NUCLEON F_2^p

We first show the numerical results of $F_2^p(x, Q^2)$ at the small- x . To carry out the numerical calculations, it is necessary to determine the parameters of the model, ρ and g_0^2 . The parameter ρ plays a role to fix the energy dependence of the cross section. We find $\rho = 0.845$ for the conformal case, $\rho = 0.799$ for the hard-wall case. The parameter g_0^2 is determined by the magnitude of the nucleon structure function. We find $g_0^2 = 1.23 \times 10^2$ and $g_0^2 = 1.25 \times 10^2$

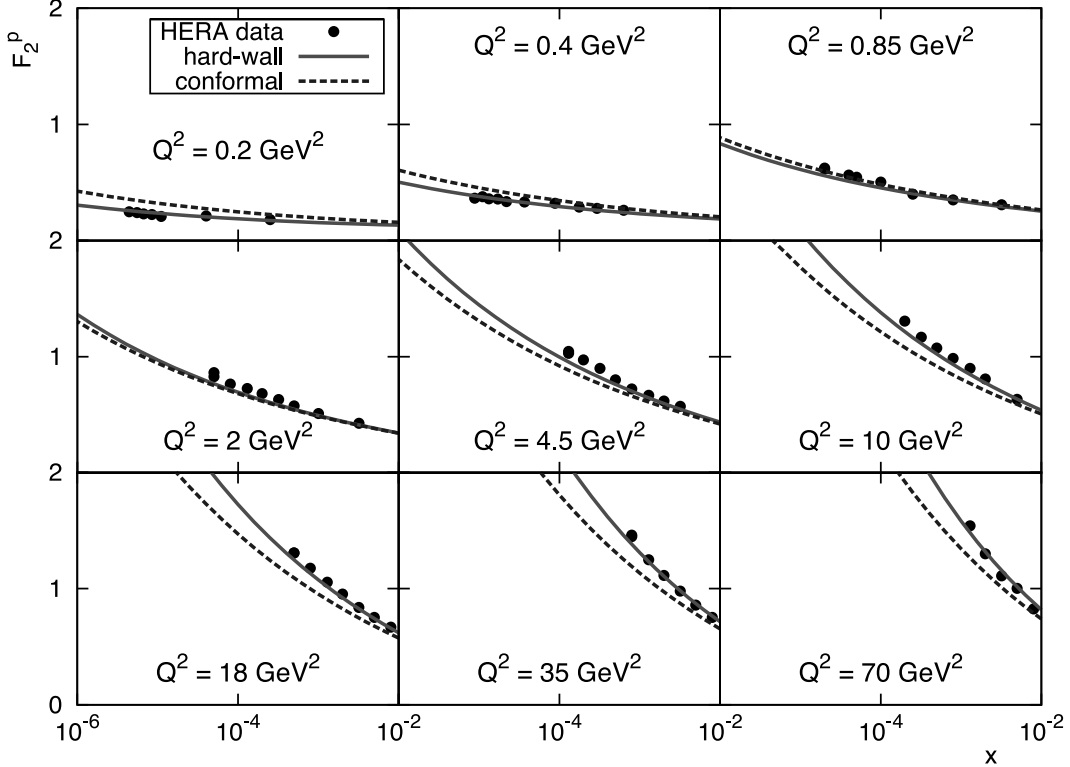


FIG. 4. $F_2^p(x, Q^2)$ as a function of the Bjorken- x for various Q^2 . In each figure, the solid and dashed curves represent results with hard-wall and conformal kernels, respectively. HERA data [33] is depicted by circles.

for the conformal and hard-wall cases, respectively. There exist additional parameters, the infrared sharp cutoff z_0 , in the hard-wall model. For the pion and the nucleon, they are determined to reproduce the pion decay constant and the nucleon mass, $z_0^\pi = 1/(322\text{MeV})$ and $z_0^N = 1/(245\text{MeV})$, respectively [11, 30]. We also introduce the hard-wall cutoff for the virtual photon in Eq. (12). This parameter is chosen to be $z_0 = 6\text{GeV}^{-1}$ to reproduce the DIS data.

We first show in Fig. 4 $F_2^p(x, Q^2)$ as a function of x for various Q^2 . At low Q^2 , F_2^p is rather insensitive to the variation of x . However, as Q^2 increases, $F_2^p(x)$ rapidly grows at the small- x region. Calculated results are in good agreement with the HERA data [33].

If we describe F_2^p at the low- x using the Pomeron exchange with the intercept α_0 , the structure function behaves as $F_2^p \sim x^{1-\alpha_0}$. From our results in Fig. 4 it is easy to recognize that the Pomeron intercept increases as Q^2 increases, which may be understood as a transition from ‘soft’ to ‘hard’ Pomerons.

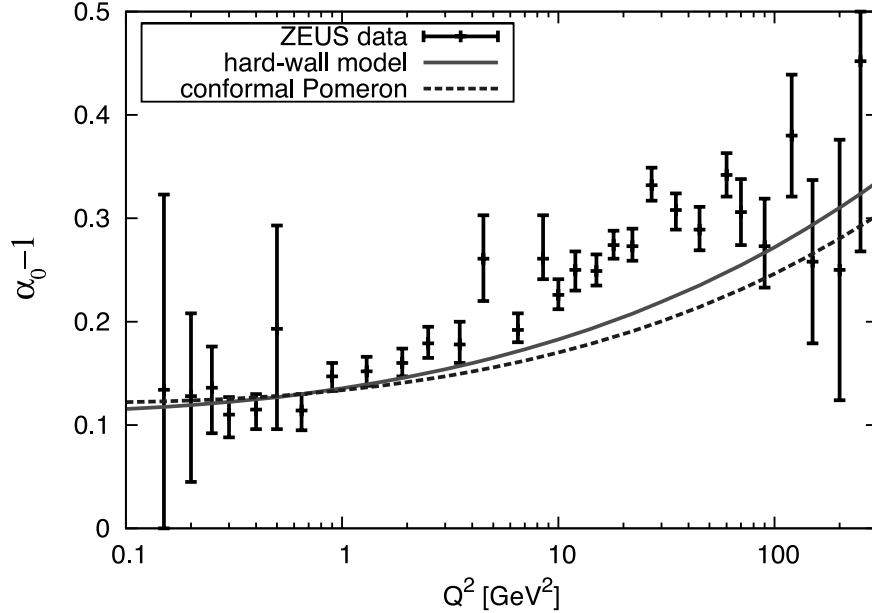


FIG. 5. The effective Pomeron intercept $\alpha_0(Q^2)$ for the nucleon. The solid and dashed curves represent results with hard-wall and conformal kernels, respectively. HERA data [3] is depicted with error bars.

To see this fact in detail, we show in Fig. 5 the effective intercept $\alpha_0(Q^2)$ extracted from the calculations of F_2^p in Fig. 4. It is evident that the grows of $\alpha_0(Q^2)$ with Q^2 increasing, although the magnitude is little bit smaller than the data [3]. For the real photon scattering at $Q^2 = 0$, the calculation shows $\alpha_0(Q^2) \sim 1.1$, which is consistent with the ‘soft’ Pomeron intercept describing the high energy scattering phenomenologically. On the other hand, $\alpha_0(Q^2)$ reaches about 1.3 at $Q^2 \sim 100\text{GeV}^2$, which is expected from the perturbative ‘hard’ Pomeron picture.

Our results are quantitatively similar with those of Ref. [18] in which the super local approximation is adopted. However, the purpose of this work is to clarify whether or not the BPST Pomeron kernel with the AdS wave functions calculated from the holographic QCD describe the DIS structure function in both soft and hard Q^2 regions. The present results show our framework based on the holography indeed works well to reproduce the nucleon structure function and account for the scale dependence of the Pomeron intercept without any artificial assumptions.

Size of the effects introduced by the hard-wall cutoff for the BPST Pomeron kernel is seen in Fig. 4 by the solid curve to be compared with the conformal case (dashed curve).

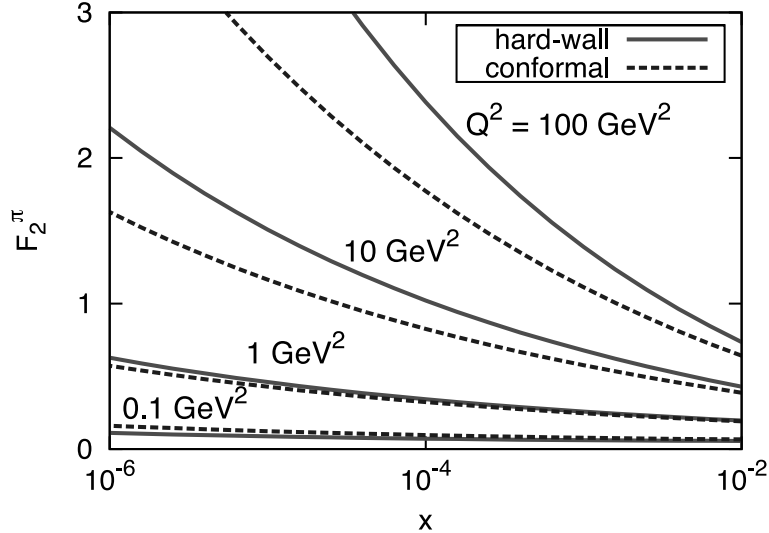


FIG. 6. $F_2^\pi(x, Q^2)$ for $Q^2 = 0.1, 1, 10, 100\text{GeV}^2$ are shown as a function of x . The solid and dashed curves show the hard-wall and conformal results, respectively.

Whereas the hard-wall results are somewhat smaller than those of the conformal kernel at lower Q^2 , the calculation of the hard-wall model exceeds the conformal cases at the higher Q^2 region. This behavior certainly depends on the choice of the parameters, especially ρ . If we used the same values of ρ and g_0 for both the hard-wall and conformal models, the solid curve would tend to agree with the dashed one at the $Q^2 \rightarrow \infty$ limit. In any case, the hard-wall model is more sensitive to the variation of Q^2 , and thus adequate to account for the soft to hard transition of the Pomeron.

V. RESULTS FOR PION STRUCTURE FUNCTION F_2^π

We then apply the same framework to the pion structure function F_2^π . The experimental information is not enough to understand the small- x behavior of the pion structure function, because one cannot perform the deep inelastic scattering with the pion target. The valence quark distribution of the pion is relatively well determined by using the Drell-Yan process [34, 35]. However, recent reanalysis with the resummation technique indicates there still exist ambiguities of the shape of the valence distribution [36]. Moreover, the sea quark and gluon distributions are ill determined. In our approach, we predict F_2^π at the small- x without any adjustable parameter, once the model parameters, ρ, g_0 , are fixed by the nucleon data.

In Fig. 6 we show the x -dependence of $F_2^\pi(x, Q^2)$ for various Q^2 . At $Q^2 = 0.1\text{GeV}^2$, where

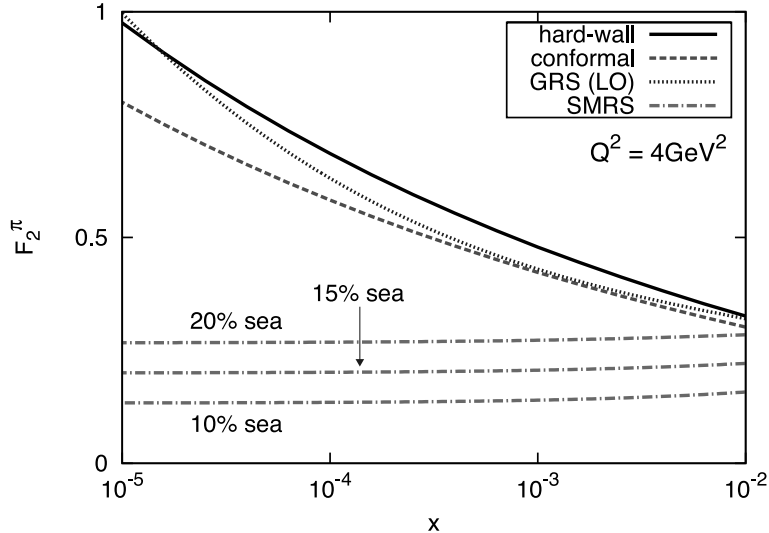


FIG. 7. $F_2^\pi(x, Q^2)$ at $Q^2 = 4\text{GeV}^2$. The solid and dashed curves show the conformal and hard-wall results, respectively. The SMRS [34] and GRS [35] parameterizations are depicted by the dash-dotted and dotted curves, respectively.

non-perturbative dynamics dominates, the structure function is almost constant. With the virtuality Q^2 increasing, the x -dependence becomes steeper, which is already seen in the nucleon case. In Fig. 7 the calculations at $Q^2 = 4\text{GeV}^2$ are compared with SMRS [34] and GRS [35] parameterizations of the pion structure function, and shown to be significantly different from them. However, we could not draw strong conclusion from this comparison, since the parameterization of F_2^π at the small x contains uncertainties as already mentioned.

The effective Pomeron intercept is also calculated for the pion case, shown in Fig. 8. Both magnitude and Q^2 -dependence are similar with the nucleon case, which may indicate the universality of the Pomeron intercept for various hadrons.

There also exist experimental information on the pion structure function from a forward neutron production in the semi-inclusive deep inelastic scattering off the nucleon [19] as illustrated in Fig. 9. This process could be understood as a convolution of the deep inelastic lepton pion scattering cross section with the momentum distribution of the pion produced by the πpn interaction in Fig. 10, if there is a large rapidity gap between jets from the pion and the forward neutron.

The cross section of the semi-inclusive $e + p \rightarrow e' + n + X$ process is assumed to be given

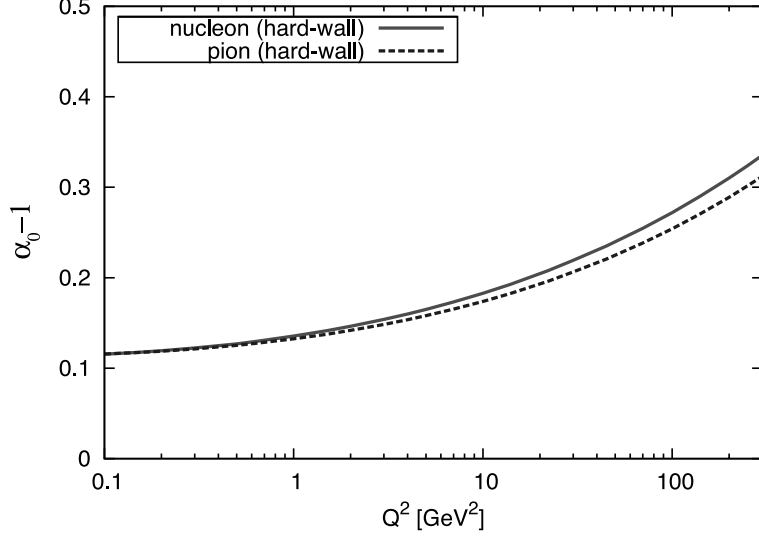


FIG. 8. The effective Pomeron intercept $\alpha_0(Q^2)$ for the pion (dashed curve) is shown with the nucleon result (solid curve).

by

$$d\sigma(ep \rightarrow e'nX) = f_{\pi^+/p}(x_L, t) \cdot d\sigma(e\pi^+ \rightarrow e'X) , \quad (42)$$

where $f_{\pi^+/p}$ is the pion flux from the nucleon, x_L the longitudinal momentum fraction carried by the leading neutron, and t the 4-momentum transfer to the pion. The flux can be calculated with the standard pion-nucleon interaction in the infinite momentum frame [37];

$$f_{\pi^+/p}(x_L, t) = \frac{1}{2\pi} \frac{g_{p\pi n}^2}{4\pi} (1 - x_L) \frac{-t}{(m_\pi^2 - t)^2} \exp\left(-R_{\pi n}^2 \frac{m_\pi^2 - t}{1 - x_L}\right) , \quad (43)$$

where m_π is the pion mass, the coupling constant $g_{p\pi n}^2/4\pi = 13.6$, and the exponential form factor with $R_{\pi n} = 0.93 \text{ GeV}^{-1}$ [37]. Integrating $f_{\pi^+/p}$ over the momentum transfer, we obtain the pion flux from the nucleon as

$$\Gamma_\pi(x_L) = \int_{t_0}^{t_{\min}} f_{\pi^+/p}(x_L, t) dt , \quad (44)$$

where

$$t_{\min} = -(1 - x_L) \left(\frac{m_n^2}{x_L} - m_p^2 \right) , \quad (45)$$

$$t_0 = -\frac{(p_T^{\max})^2}{x_L} + t_{\min} . \quad (46)$$

We set $x_L = 0.73$ and $p_T^{\max} = 0.2 \text{ GeV}$ from HERA data [19]. Resulting pion flux yields 0.133, although this value contains non-negligible errors due to uncertainties of the measured x_L

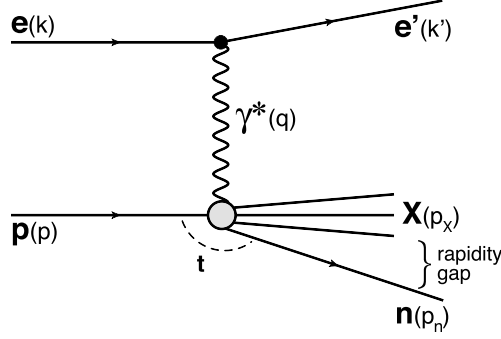


FIG. 9. The forward neutron production with the large rapidity gap by γ^*p scattering.

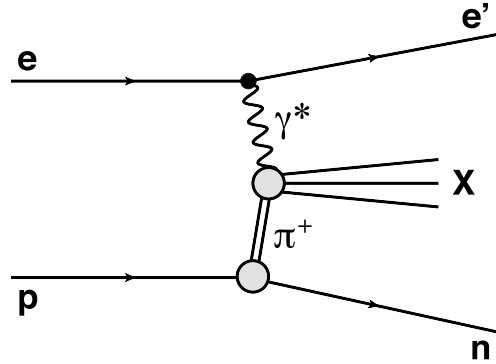


FIG. 10. The forward neutron production with the pion exchange model.

and p_T . There may be additional contributions from the Δ mediated process, $p \rightarrow \Delta\pi$ [38], which we do not take into account in this work.

Using our calculation for F_2^π , we compare the results with the experimental data in Fig. 11. Because this analysis depends on the inputs of x_L and p_T in Eq. (44), absolute magnitudes of the calculations involve theoretical errors which may be about 30% at most. Hence, our results are consistent with the experimental data qualitatively.

VI. SUMMARY AND DISCUSSIONS

We have calculated the nucleon and pion structure functions at the small- x and studied the interplay between the soft and hard Pomerons in terms of the holographic QCD. The structure function at the small- x is given by a convolution of the BPST Pomeron exchange kernel $\chi(s, z, z')$ with overlap functions of the virtual photon $P_{13}(z, Q^2)$ and the target hadron $P_{24}(z')$ in the AdS space. We have emphasized the behavior of $P_{13}(z)$ and $P_{24}(z')$ in the AdS space is a key to determine the value of the Pomeron intercept. Only when the peak

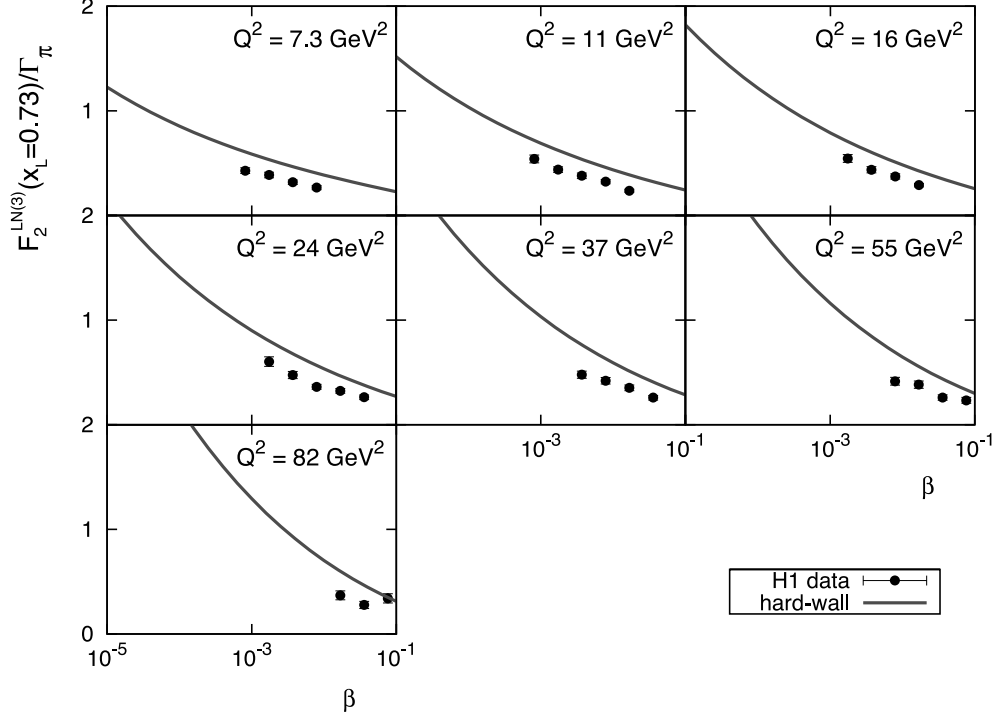


FIG. 11. The forward neutron production in the semi-inclusive DIS. Our calculation and the experimental data [19] are shown by the solid curves and circles, respectively.

position of $P_{13}(z, Q^2)$ in the z -space is away from the distribution of $P_{24}(z')$ in the z' -space, the resulting Pomeron intercept α_0 is enhanced. This tendency is demonstrated by the super local (delta function) approximation for the overlap functions in Sec. II.

To be realistic, we have calculated the wave functions of the nucleon and the pion, which are the solutions of the classical action in the AdS space, and evaluated their couplings to the Pomeron. The Pomeron(graviton)-hadron-hadron coupling can be calculated by perturbing the metric in the classical action, and are essentially proportional to the square of the holographic wave functions in the AdS space.

As already known, the photon part $zP_{13}(z)$ has a flat distribution in the AdS z space at $Q^2 \sim 0$, while it shows a sharp peak at $z = 0$ for $Q^2 \gg 1\text{GeV}^2$. On the other hand, overlap functions $P_{24}(z')$ of the nucleon and the pion are shown to be concentrated in the larger z' region, near the hard-wall cutoff z_0 . Such a behavior of the overlap functions are consistent with what we require to describe the transition between soft and hard Pomerons.

With these inputs we have calculated the nucleon structure function $F_2^p(x, Q^2)$ at the low- x . The results fairly agree with the experimental data. In particular, Q^2 dependence of

the effective Pomeron intercept $\alpha_0(Q^2)$ is consistent with the data, namely, the value of the Pomeron intercept α_0 increases from the soft value 1.1 to the hard one 1.3 as the photon virtuality Q^2 increases from non-perturbative to the perturbative regions.

In general, our results are very similar with Ref. [18] where *ad hoc* super local (delta function) approximation is used for the overlap functions. Nevertheless, our work is the first attempt to calculate the nucleon structure function at the small- x with the holographic QCD in a systematic way. The present approach enables us to calculate the scattering cross section of various hadrons without additional free parameters by evaluating their distributions in the AdS space.

We have newly calculated the pion structure function $F_2^\pi(x, Q^2)$ in this model. The resulting pion structure function at the small- x is reduced by about 30% in magnitude compared with the nucleon case. Unfortunately, we could not compare our calculations with the data, because the existing parameterizations of the pion structure function may already include large errors. However, the semi-inclusive DIS with a forward neutron production provides (model dependent) constraints on the pion structure function, if one assume the pion exchange model for this process. Our calculations are consistent with the data within theoretical uncertainties.

Because of the lack of experimental information on $F_2^\pi(x, Q^2)$, a simple relation between nucleon and pion structure functions is often used to estimate $F_2^\pi(x, Q^2)$ as [39, 40],

$$F_2^\pi(x, Q^2) \simeq \frac{2}{3} F_2^p\left(\frac{2}{3}x, Q^2\right). \quad (47)$$

This relation simply originates from the difference of the number of the valence quarks in the pion and the nucleon, although it is questionable whether or not this relation can be applied to the small- x region, at which the gluon dominates.

We show in Fig. 12 the calculated pion F_2^π by the solid curve (LHS of Eq. (47)) and a result calculated by the scaling relation (47) with the input of the calculated nucleon F_2^p (RHS of (47)). It is interesting to see this relation is satisfied almost perfectly, although we cannot explain why it holds within our framework.

It is our strong desire to extend the present approach to the hadron-hadron scattering. In this case, the scattering amplitude of hadrons i and j is given by

$$\mathcal{A}(s, t) = 2is \int d^2b e^{i\mathbf{q}\cdot\mathbf{b}} \int dz dz' P_i(z) P_j(z') \{1 - e^{i\chi(s, b, z, z')}\}. \quad (48)$$

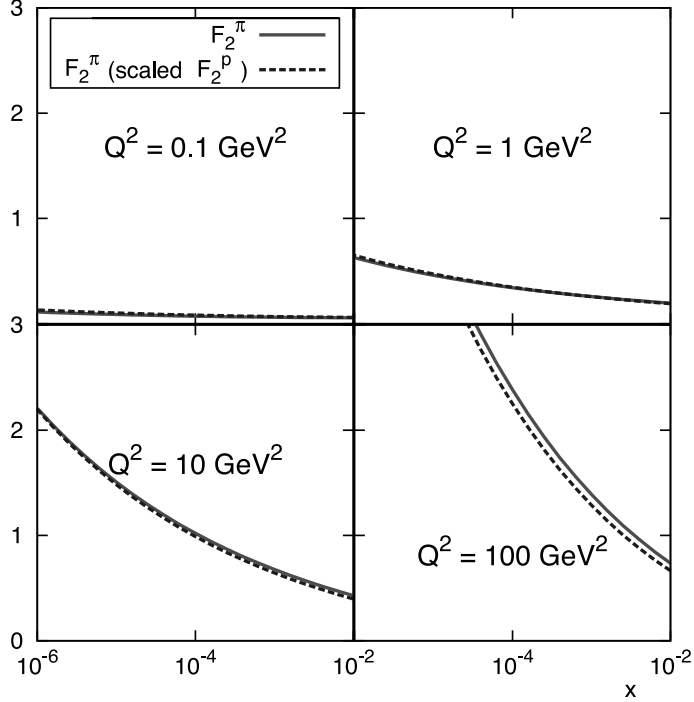


FIG. 12. Calculated F_2^π (solid curve) from holography and the result with the scaling relation Eq. (47) (dashed curve).

If i and j are the same hadron, $P_i(z)$ and $P_j(z')$ have the same distribution in z and z' spaces, respectively. According to our results for DIS, the Pomeron intercept α_0 becomes small (soft) in case the distribution of the incident and target particles are similar. Therefore, we expect the hadron scattering of the identical particles can be described by the soft Pomeron, which is consistent with the phenomenologies. Even if we consider the hadron scattering of the different species, shapes of $P_i(z)$ and $P_j(z')$ in the AdS space are not so different. Thus, we also expect the hadron scattering of different particles to be described by the soft Pomeron exchange. These studies are now in progress.

Another possible extension of this work is to consider the diffractive photo- and lepto-production of neutral vector mesons, ρ , ϕ , J/ψ , Υ [5]. Experimental data of these processes also clearly show the scale dependence of the Pomeron intercept. In this case, the quark mass as well as the photon virtuality play roles of the hard scale, In order to apply our framework, it is necessary to evaluate the photon-Pomeron-vector meson coupling in the AdS space, which is under considerations.

ACKNOWLEDGMENTS

A.W. acknowledges G. Ogawa for useful comments on the holographic description of the nucleon. We also thank all the members of the quark/hadron group in Tokyo University of Science for useful conversations.

-
- [1] See, *e. g.* J. R. Forshaw and D. A. Ross, "Quantum Chromodynamics and the Pomeron", (Cambridge University Press, London, 1997).
 - [2] A. Donnachie and P. V. Landshoff, Phys. Lett. **B470**, 243 (1999).
 - [3] J. Breitweg *et al.* [ZEUS Collaboration], Eur. Phys. J. C **7**, 609 (1999) [arXiv:hep-ex/9809005].
 - [4] E.A. Kuraev, L.N. Lipatov and V.S. Fadin, Sov. Phys. JETP **45** (1977), 199; Ya.Ya. Balitsky and L.N. Lipatov, Sov. J. Nucl. Phys. **28** (1978), 22.
 - [5] For a review, I. P. Ivanov, N. N. Nikolaev and A. A. Savin, Phys. Part. Nucl. **37**, 1 (2006) [hep-ph/0501034], and references therein.
 - [6] J. M. Maldacena, Adv. Theor. Math. Phys. **2**, 231 (1998) [Int. J. Theor. Phys. **38**, 1113 (1999)] [hep-th/9711200].
 - [7] S. S. Gubser, I. R. Klebanov and A. M. Polyakov, Phys. Lett. B **428**, 105 (1998) [hep-th/9802109].
 - [8] E. Witten, Adv. Theor. Math. Phys. **2**, 253 (1998) [hep-th/9802150].
 - [9] O. Aharony, S. S. Gubser, J. M. Maldacena, H. Ooguri and Y. Oz, Phys. Rept. **323**, 183 (2000) [hep-th/9905111].
 - [10] D. T. Son and M. A. Stephanov, Phys. Rev. D **69**, 065020 (2004) [hep-ph/0304182].
 - [11] J. Erlich, E. Katz, D. T. Son and M. A. Stephanov, Phys. Rev. Lett. **95**, 261602 (2005) [hep-ph/0501128].
 - [12] J. Polchinski and M. J. Strassler, Phys. Rev. Lett. **88**, 031601 (2002) [hep-th/0109174].
 - [13] J. Erdmenger, N. Evans, I. Kirsch and E. Threlfall, Eur. Phys. J. A **35**, 81 (2008) [arXiv:0711.4467 [hep-th]].
 - [14] For reviews, J. Erlich, PoS CONFINEMENT **8**, 032 (2008) [arXiv:0812.4976 [hep-ph]], J. Erlich, Int. J. Mod. Phys. A **25**, 411 (2010) [arXiv:0908.0312 [hep-ph]].
 - [15] R. C. Brower, J. Polchinski, M. J. Strassler and C. -I. Tan, JHEP **0712**, 005 (2007)

- [hep-th/0603115].
- [16] R. C. Brower, M. J. Strassler and C. -I. Tan, JHEP **0903**, 050 (2009) [arXiv:0707.2408 [hep-th]].
- [17] R. C. Brower, M. J. Strassler and C. -I. Tan, JHEP **0903**, 092 (2009) [arXiv:0710.4378 [hep-th]].
- [18] R. C. Brower, M. Djuric, I. Sarcevic and C. -I. Tan, JHEP **1011**, 051 (2010) [arXiv:1007.2259 [hep-ph]].
- [19] F. D. Aaron *et al.* [H1 Collaboration], Eur. Phys. J. C **68**, 381 (2010) [arXiv:1001.0532 [hep-ex]].
- [20] J. Polchinski and M. J. Strassler, JHEP **0305**, 012 (2003) [hep-th/0209211].
- [21] Y. Hatta, E. Iancu and A. H. Mueller, JHEP **0801**, 026 (2008) [arXiv:0710.2148 [hep-th]].
- [22] E. Levin, J. Miller, B. Z. Kopeliovich and I. Schmidt, JHEP **0902**, 048 (2009) [arXiv:0811.3586 [hep-ph]].
- [23] M. Henningson and K. Sfetsos, Phys. Lett. B **431**, 63 (1998) [hep-th/9803251].
- [24] W. Muck and K. S. Viswanathan, Phys. Rev. D **58**, 106006 (1998) [hep-th/9805145].
- [25] R. Contino and A. Pomarol, JHEP **0411**, 058 (2004) [hep-th/0406257].
- [26] D. K. Hong, T. Inami and H. -U. Yee, Phys. Lett. B **646**, 165 (2007) [hep-ph/0609270].
- [27] H. J. Kwee and R. F. Lebed, JHEP **0801**, 027 (2008) [arXiv:0708.4054 [hep-ph]].
- [28] H. R. Grigoryan and A. V. Radyushkin, Phys. Rev. D **76**, 115007 (2007) [arXiv:0709.0500 [hep-ph]].
- [29] H. R. Grigoryan and A. V. Radyushkin, Phys. Rev. D **77**, 115024 (2008) [arXiv:0803.1143 [hep-ph]].
- [30] Z. Abidin and C. E. Carlson, Phys. Rev. D **79**, 115003 (2009) [arXiv:0903.4818 [hep-ph]].
- [31] Z. Abidin and C. E. Carlson, Phys. Rev. D **77**, 115021 (2008) [arXiv:0804.0214 [hep-ph]].
- [32] H. R. Grigoryan and A. V. Radyushkin, Phys. Rev. D **78**, 115008 (2008) [arXiv:0808.1243 [hep-ph]].
- [33] F. D. Aaron *et al.* [H1 and ZEUS Collaboration], JHEP **1001**, 109 (2010) [arXiv:0911.0884 [hep-ex]].
- [34] P. J. Sutton, A. D. Martin, R. G. Roberts and W. J. Stirling, Phys. Rev. D **45**, 2349 (1992).
- [35] M. Gluck, E. Reya and I. Schienbein, Eur. Phys. J. C **10**, 313 (1999) [hep-ph/9903288].
- [36] M. Aicher, A. Schafer and W. Vogelsang, Phys. Rev. Lett. **105**, 252003 (2010) [arXiv:1009.2481

[hep-ph]].

- [37] H. Holtmann, G. Levman, N. N. Nikolaev, A. Szczurek and J. Speth, Phys. Lett. B **338**, 363 (1994).
- [38] A. W. Thomas and C. Boros, Eur. Phys. J. C **9**, 267 (1999) [hep-ph/9812264].
- [39] N. N. Nikolaev, J. Speth and V. R. Zoller, Phys. Lett. B **473**, 157 (2000) [hep-ph/9911433].
- [40] S. Chekanov *et al.* [ZEUS Collaboration], Nucl. Phys. B **637**, 3 (2002) [hep-ex/0205076].